

Processing Of Mammographic Images Using Speckle Technique

A.M. Hamed¹ and Tarek A. Al-Saeed²

¹Physics Dept., Faculty of Science, Ain Shams University, 11566 Cairo, Egypt.

²Biomedical Eng., Faculty of Engineering, Helwan University, Cairo, Egypt.

ABSTRACT

We study the malignant and benign mammographic x – ray images using speckle techniques. Discrimination between the mammographic images is outlined using circular aperture segmentation. The algorithm is based on the selection of the interested segment from the mammographic image. We multiply the segment by a uniform circular aperture of diameter nearly equal the dimensions of the segment. Then, we multiply the modulated segment by a diffuse function. Finally, we operate the Fourier transform upon the three matrices to get a modulated speckle images. These modulated images are dependent upon the information on the selected image segment. The modulated speckle images and profiles of the mammographic images are investigated using mat-lab code.

Key Words: Mammographic x- ray images; modulated speckle images; correlation and contours of benign and malignant images.

I. INTRODUCTION

Physicians are interested to have more information about medical images. One branch of imaging uses the optical and laser microscopy which is useful to examine the blood cells and plasma. The other branch based on x– ray, ultra sonic, and MRI imaging is useful to get more information since the resolution limit is improved in the direction of frequency increase. In all cases of imaging, it is recommended to make image processing to get more information and details [1-4]. For this reason, we make this study to distinguish between the normal, benign, and malignant mammographic images using speckle techniques and correlation [5-12]. In this study, the algorithm is based on speckle image formation modulated by the former mammographic images in presence of randomly distributed function as a diffuser. The speckle images are compared with the corresponding speckle image in absence of the former image. Another comparative technique based on correlation is investigated. A circular aperture modulation is used during the formation of the above speckle images. Also, two circular apertures are proposed in the formation of speckle of mammographic image and diffuser giving a grid structure which facilitates the distinction between images. All speckle images and the grid structure of speckle images are investigated giving better information in case of grid structure.

II. THEORETICAL ANALYSIS

In this analysis, we represent the x- ray mammographic image by a function $f(x, y)$. It is written in a discrete form as a matrix of dimensions $M \times N$ as follows:

$$f(x, y) = \sum_{m=1}^M \sum_{n=1}^N f(m\Delta x, n\Delta y) \quad (1)$$

Where Δx and Δy are the rectangle widths of the image and matrix dimensions are taken as $M=1024$ and $N= 1024$. For the image of dimensions 4cm^2 , $\Delta x = \Delta y = 2 \mu\text{m}$.

Now a circular uniform aperture is used in the segmentation process, it is represented as follows:

$$A(x, y) = 1 ; \left| \frac{\rho}{\rho_0} \right| \leq 1 \quad (2)$$

Where (x, y) has the same dimensions like the image matrix of 1024×1024 pixels and the radial coordinate is $\rho_0 = (x^2 + y^2)^{1/2}$ is 64 pixels.

The diffuser has a randomly distributed function represented as $d(x, y)$ and has the same dimensions like the above matrices. It is used to fabricate the ordinary speckle image in case of uniform circular aperture and in absence of the image. Now, the multiplication of the three matrices in the same sequence will give a new matrix of same dimensions like the other matrices.

The result is represented as follows:

$$B(x, y) = f(x, y).A(x, y).d(x, y) \tag{3}$$

The Fourier transform is operated upon the multiplication product to get this convolution product:

$$B(u, v) = F.T. [f(x, y).A(x, y).d(x, y)],$$

$$\tilde{B}(u, v) = \tilde{f}(u, v) * \tilde{A}(u, v) * \tilde{d}(u, v) \tag{4}$$

Referring to the convolution theorem, the simple product of the three matrices is transformed into convolution product. For example, $\tilde{f}(u, v) = F.T. [f(x, y)]$, etc.

In case of one circle, we substitute equation (2) in equation (3) and solve for the transformation to get:

$$\tilde{B}(u, v) = 2 * \left[\frac{J_1(w)}{w} \right] * \tilde{f}(u, v) * \tilde{d}(u, v) \tag{5}$$

$w = (2\pi \rho_0/\lambda f) (u^2 + v^2)^{1/2}$ is the reduced coordinate in the Fourier plane (u, v). λ is the wavelength of laser radiation and f is the focal length of the Fourier transform lens.

Also, two circular apertures are proposed for the modulation, and we get a grid structure of the speckle image in the following form:

$$\tilde{B}(u, v) = \cos(w) * \tilde{f}(u, v) * \tilde{d}(u, v) \tag{6}$$

It is noted that w has a dimensionless value as stated in equation (5).

III. WHAT IS BREAST CANCER

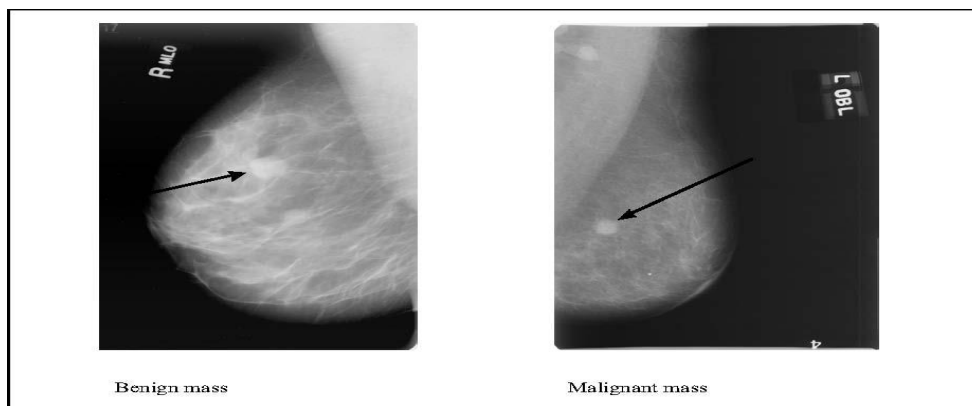
Breast cancer is a “malignant neoplasm of the breast.” A cancer cell has characteristics that differentiate it from normal tissue cells with respect to: the cell outline, shape, structure of nucleus and most importantly, its ability to metastasize and infiltrate. When this happens in the breast, it is commonly termed as ‘Breast Cancer’. Cancer is confirmed after a biopsy (surgically extracting a tissue sample) and pathological evaluation.

IV. MORPHOLOGIC PRESENTATIONS

As you can see from the mammograms and diagrams, the breast tissue comprises of small intricate structures so pathology can easily be overlooked, especially if the film quality is not good. Not all structures are cancers. Many structures or macro (big) calcifications are often benign. Some basic forms of pathology and morphology presentations are (Addendum 3):

Masses and Densities

Masses’ differ from ‘Densities’ because ‘masses’ are seen on two views whereas ‘densities’ are seen on one view only. Hence, two views of each breast to identify this abnormality. Masses with smooth rounded edge are generally a fluid-filled cyst that can be confirmed by an ultrasound and aspirated to relieve pain for the woman. Hard lesions with uneven edges might be reason for follow-up procedures. A mass could be palpable (can feel it during a physical breast exam) depending on the size and proximity to the skin surface. A fat containing mass looks radiolucent on the mammogram. Sometimes, it is very difficult for radiologists to differentiate between a benign and a malignant mass off mammograms (as in Fig. below), so additional imaging modalities and/or biopsy may be required.



Examples of benign mass and a malignant mass Ref. [*]

Micro calcifications

Calcifications are small calcium deposits that can be detected on a mammogram. Minute calcifications are called micro calcifications and bigger ones are called macro calcifications. The latter is generally benign and does not need additional follow-up. Sometimes, other structures mimic micro calcifications such as calcified arteries that appear like ‘train tracks’. This is normal. Artifacts on mammograms due to specs of dust may look like micro calcifications, but the difference is that these specs are bright and shiny whilst a micro calcification looks ‘milky white’. Radiologists categorize the calcifications as malignant or benign based on (1) the location of calcifications, (2) the arrangement (linear or scattered or clusters) (3) the total number of micro calcifications (4) the changes with respect to the previous mammograms.

Quantitative results

The mammographic images shown in the figure (1) are investigated using speckle imaging and the correlation techniques. The basic differentiation of the x-ray mammographic images is outlined in the above section of morphological presentations.

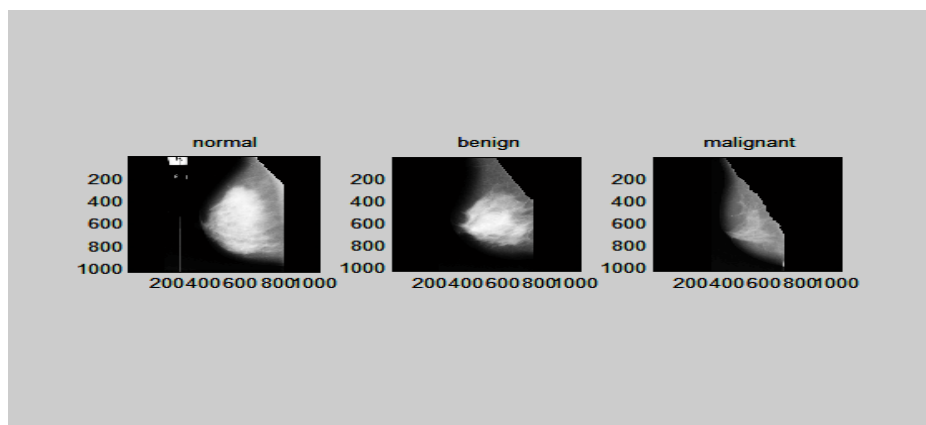


Figure (1): Three mammographic images each have the same matrix dimensions 1024x1024 pixels. As shown from the left is the **normal** mammogram” mdb003”, in the middle **circular benign masses** are shown “mdb001”, while in the right a **malignant micro-calcification** is shown in the image “mdb213”.

Now, referring to the figure (2), X1, X2, X3 represent the contour images of the normal, benign, and malignant images as illustrated in the 1st row. In the graph, X1 has shown uniform elliptic shape in the range from (800,600) up to (300, 700) while for the benign image X2, hallow is concentrated in the range from (700,500) up to (800,450) around the center. The malignant image showed a deformed triangular shape. In the 2nd row three contour images are shown. The 1st represent the autocorrelation X11 of the normal image X1 which has a nearly isotropic shape while the cross correlation of the normal image X1 and benign image X2 is X12 has shown asymmetric shape. Finally, the cross correlation of the malignant image X3 with the normal image X1 has shown an elongation along y axis and deformed from the left which its contour X13 has a different shape as compared with the other correlation contours X11 and X12.

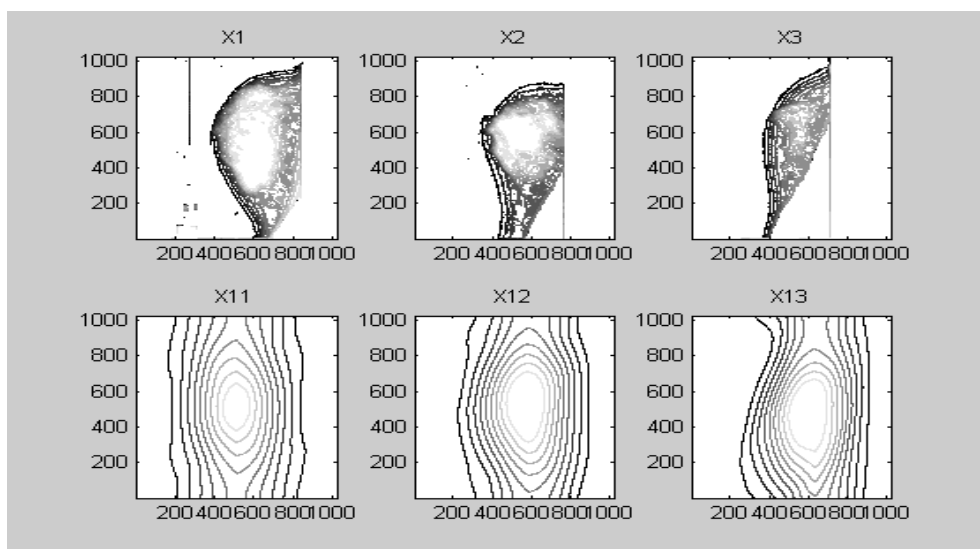


Figure (2): The contour of the original images X1, X2, X3 is plotted in the 1st row and the contour of the autocorrelation image X11 and the cross correlation images X12, X13 are shown in the 2nd row. Ten contour lines are shown for all images.

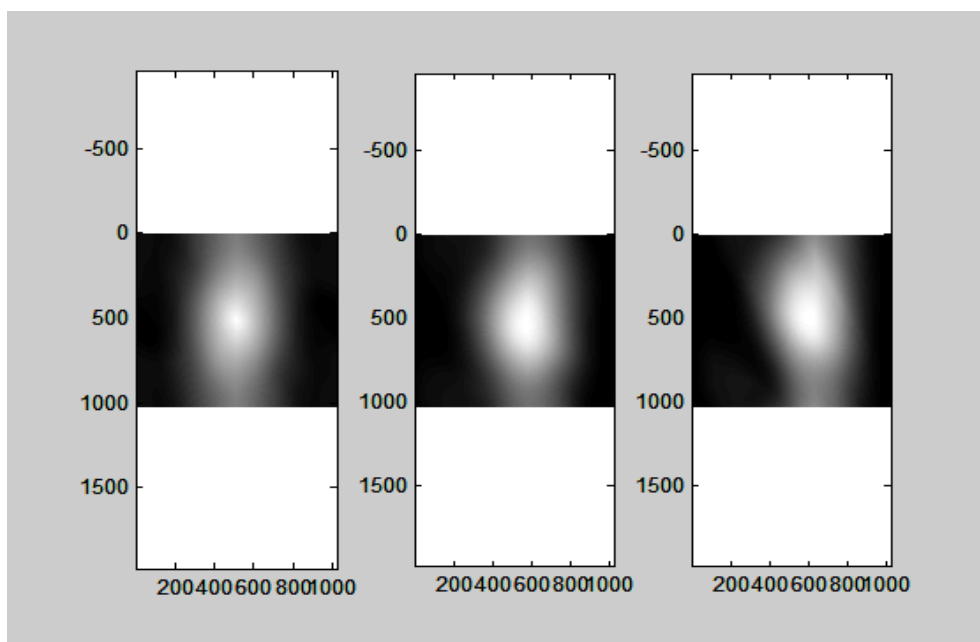


Figure (3): In the left photo, the autocorrelation image corresponding to the normal mammographic image shown, a cross correlation image for the normal and benign images is shown in the middle. In the right, the cross correlation image for the normal and malignant images is shown.

As shown in figure (3): X11 is the autocorrelation profile of the image X1 i.e. $X11 = X1 \otimes X1$, and X12, X13 represent the profiles of the cross correlation images, $X12 = X1 \otimes X2$, $X13 = X1 \otimes X3$.

The correlation product symbol is represented as \otimes .

It is shown that X11 for the normal mammogram has a symmetric distribution and a sharp peak while both of the benign and malignant profiles X12, X13 have a curved shape around the peak. Referring to the correlation images as shown in figure (3), the autocorrelation of the normal image has shown isotropic shape, the cross correlation of the normal and benign images showed more curvature to the left. The last cross correlation of the normal with the malignant images showed more curvature to the left. Hence, the cross correlation images showed an intense bright hallow in a wider region around the center as compared with the sharp spot appeared in the autocorrelation image.

The figure (4), ten horizontal section of the above correlation images are plotted giving the isotropic autocorrelation profiles for the normal image as in figure (4 – a) while the cross correlation plots with the benign and malignant images are shown in figures (4-b, c). All profiles are taken for horizontal lines at 512,450,400,350,300,250,200,150,100,50 pixels. It is shown, as in figure (4-a), that the ten curves have invariant peak at 512 pixels. This expected result is due to the symmetry originated from the autocorrelation. Contrarily to this result the ten curves appeared in the cross correlation, as in figures (4 – b, c), showed a variable peak shifted to 600 pixels for the horizontal line at 300 pixels figure (4-b) and shifted to 650 pixels for the same horizontal line at 300 pixels figure (4-c). The band width at half maximum (BWHM) of the correlation plots at the center of the pattern is calculated as follows:

$BW_1 = 343 \text{ pixels}$; *BWHM for the autocorrelation of the normal image.*

$BW_2 = 388 \text{ pixels}$; *BWHM for the cross correlation with the benign image.*

$BW_3 = 400 \text{ pixels}$; *BWHM for the cross correlation with the malignant image.*

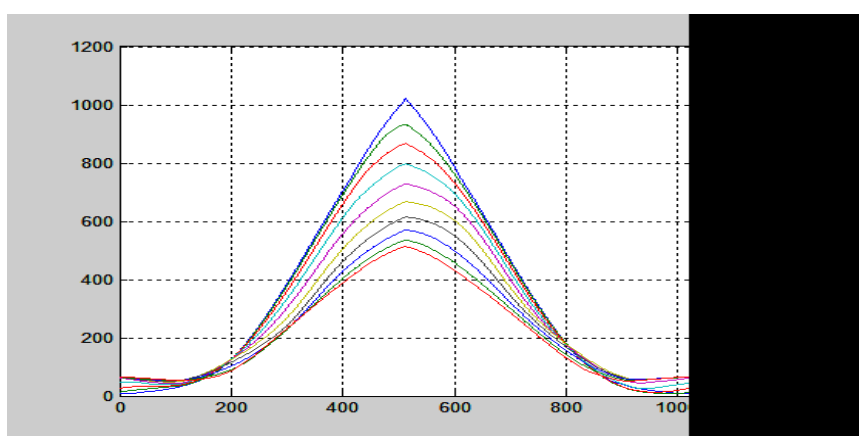


Figure (4- a): Plot of the autocorrelation profiles X11 for horizontal lines at 512,450,400,350,300,250,200,150,100,50 pixels.

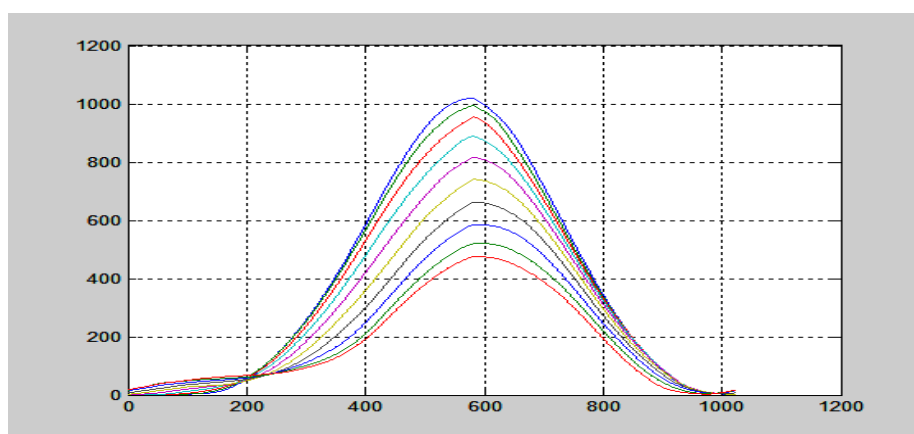


Figure (4- b): Plot of the cross correlation profiles X12 for horizontal lines at 512,450,400,350,300,250,200,150,100,50 pixels.

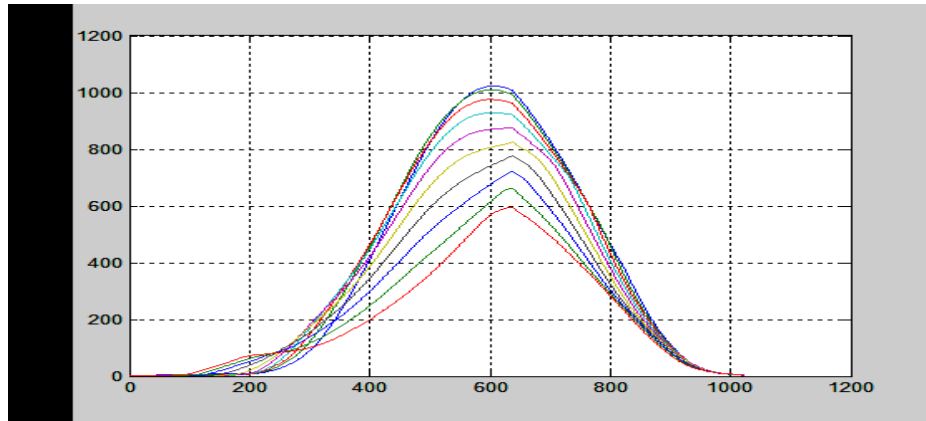


Figure (4 - c): Plot of the cross correlation profiles X13 for horizontal lines at 512,450,400,350,300,250,200,150,100,50 pixels.

Referring to the obtained speckle images calculated from equation (5) are represented as in figure (5 – a), we observe that more luminous spots are appeared in case of benign and malignant images as compared with the normal mammographic image. These luminous spots which discriminates one image from the other with the weak patches of spots form the speckle images. In the normal image, three luminous spots are shown as compared with more than nine spots visualized in case of benign mammographic image while four spots located in a different position are seen in the malignant image. This difference between speckle images is attributed to the scattering of different luminous spots of the original images in figure (1) for certain diffuser and circular aperture with the same radius.

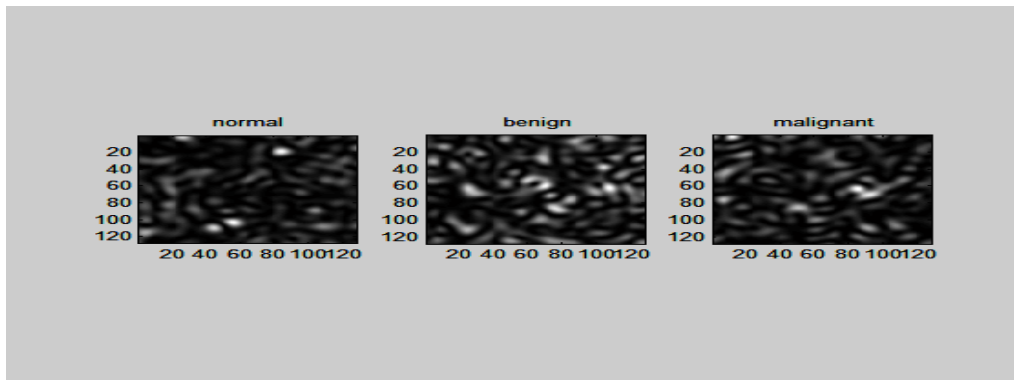
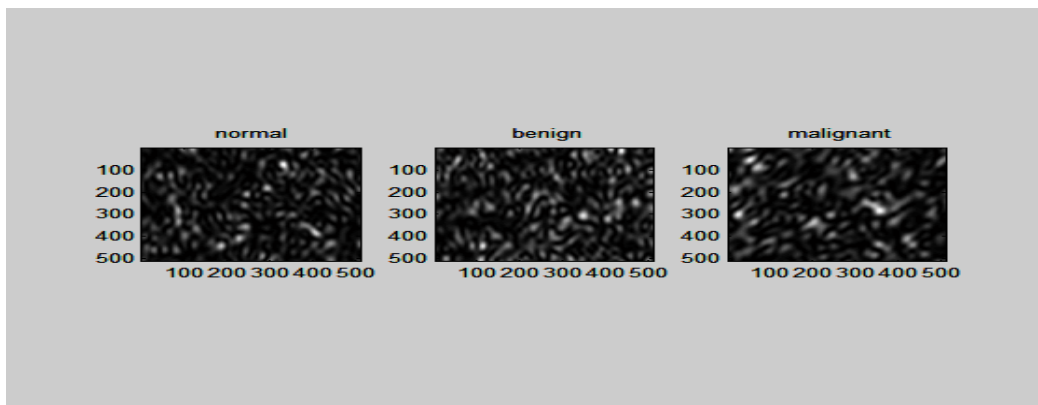


Figure (5-a): The three speckle photos are taken using a diffuser of 1024x1024 pixels and the original images are obstructed with circular aperture of radius 64 pixels. The speckle images are of dimensions 128x128.



(5 -b): Two circles used in the formation of the grid structure of speckles shown in figure (4-b).

The grid structure appeared in the speckle images shown in figure (5-b) is due to interference originated from the two displaced circles located in the object plane superposed over the diffuser. The resulting images are computed using equation (6). The grid structure originated inside the patches of the speckle images facilitates the discrimination.

V. CONCLUSION

We have used two different techniques to process the mammographic images based on speckle and correlation techniques. Firstly, the contours obtained of the correlation images showed a good discrimination between the normal, benign, and malignant mammographic images. Secondly, the different speckle images obtained using specific randomly distributed function superimposed over the investigated images gave three different images of different luminosity. This allows discriminate the images. We believe that the difference between the speckle images is due to the convolution product of the Fourier spectrum of the original images with the ordinary speckle pattern.

REFERENCES

- [1] B. Al Hadidi , M. H. Zubi , and H.N. Sulieman , "Mammogram breast cancer detection using image processing function , Information technology journal , vol. 6, pp.217-221, 2007.
- [2] L. W. Basset, V.III Manjikian, etc. , "Mammography and breast cancer screening(Review) Surg clinics of North America , pp. 775-800 , 1990.
- [3] D.B. Kopans, "The potential impact of computer-aided diagnosis on clinical mammography". Proc. of the 3rd International workshop on Digital Mammography , 35.
- [4] M. Heath, K. Kopans , etc. "Current status of the digital data base screening mammography" , Proc. of the 4th International workshop on Digital mammography, pp. 457 - 460.
- [5] M. Tebaldi, Luciano Angel Toro, Opt. Comm. vol. 182 (2000) pp. 95 – 105, New multiple aperture arrangements for speckle photography.
- [6] Luciano Angel Toro, M. Tebaldi, Opt. Comm. 192 (2001) 37 – 47, Properties of speckle patterns generated through multi- aperture pupils.
- [7] A. M. Hamed , J. Modern Opt. 56 (2009)1174 – 1181 , Numerical speckle images using modulated linear apertures : Simulation.
- [8] A. M. Hamed , J. Modern Opt. 56 (2009)1633 – 1642 , Formation of speckle images using circular obstruction.
- [9] A. M. Hamed , J. Opt. Eng. 50 (2011) 1 – 7, Discrimination between speckle images using diffusers modulated by some apertures : Simulations.
- [10] A. M. Hamed , Optics and photonics journal 1 (2011) 41-52 ,Computer generated quadratic and higher order apertures and its application on numerical speckle images.
- [11] J. W. Goodmann , "Introduction to Fourier optics and holography", Roberts & Company Publishers, Greenwood Village, United States, third ed. , 2005.
- [12] J. W. Goodman , "Statistical properties of laser speckle patterns", Springer – Verlag , New York 1984.